Journal of Sound and Vibration (2001) **245**(5), 923–946
doi:10.1006/jsvi.2001.3612, available online at http://www.idealibrary.com on IDEAL®

FLOW-INDUCED VIBRATIONS OF A LIGHT CIRCULAR CYLINDER AT REYNOLDS NUMBERS 10^3 TO 10^4

S. MITTAL AND V. KUMAR

Department of Aerospace Engineering, Indian Institute of Technology, Kanpur, UP 208 016, *India.*
E-mail: smittal@iitk.ac.in

(*Received* 1 *September* 1999, *and in final form* 5 *February* 2001)

Stabilized space–time finite-element methods are employed to investigate vortex-induced vibrations of a light circular cylinder placed in a uniform flow at Reynolds number in the range of 10^3–10^4. The governing equations for the fluid flow are the Navier–Stokes equations for incompressible flows. The cylinder is mounted on lightly damped, flexible supports and allowed to vibrate, both in the in-line and cross-flow directions under the action of aerodynamic forces. Results are presented for various values of the structural frequency of the oscillator including those that are super-harmonics of the vortex-shedding frequency for a stationary cylinder. In certain cases the effect of the mass of the oscillator is also examined. The motion of the cylinder alters the fluid flow significantly. To investigate the long-term dynamics of the non-linear oscillator, beyond the initial transient solution, long-time integration of the governing equations is carried out. For efficient utilization of the available computational resources the non-linear equation systems, resulting from the finite-element discretization of the flow equations, are solved using the preconditioned generalized minimal residual (GMRES) technique. Flows at lower Reynolds numbers are associated with organized wakes while disorganized wakes are observed at higher Reynolds numbers. In certain cases, competition is observed between various modes of vortex shedding. The fluid–structure interaction shows a significant dependence on the Reynolds number in the range that has been investigated in this article. In certain cases *lock-in* while in some other cases *soft-lock-in* is observed. The trajectory of the cylinder shows very interesting patterns including the well-known *Lissajou* figure of *8*. Several mechanisms of the non-linear oscillator for self-limiting its vibration amplitude are observed.

1. INTRODUCTION

Flow past an oscillating cylinder has received continued attention in the past few decades. In addition to being a building block in the understanding of bluff body flows it has a large number of applications in several engineering situations. Flow past an oscillating cylinder is associated with a variety of interesting phenomena. For example, a cylinder subjected to cross-flow vibrations exhibits the phenomenon of *lock-in*. The vortex-shedding frequency related to the oscillating cylinder shifts to the frequency of cylinder vibrations [1]. However, this happens only if the oscillation amplitude is larger than a certain threshold value. Lock-in is observed for a fairly wide range of cylinder vibration frequencies centered around the vortex shedding frequency for a stationary cylinder. Interestingly, the threshold amplitude, beyond which lock-in takes place, increases with the increase in difference between the vibration frequency and the vortex shedding frequency of the stationary cylinder. Lock-in is also observed for cylinders that are mounted on flexible supports and are allowed to undergo vortex-induced oscillations [2]. Another interesting phenomenon

0022-460X/01/350923 + 24 $35.00/0

associated with vortex-induced oscillations is *hysteresis*. The oscillation amplitude, for a certain range of Reynolds number and close to the outer limits of the frequencies for lock-in, depends on whether the flow speed is decreased or increased during the experiment [3]. Several explanations have been offered by researchers in the past. While some researchers attribute it to the non-linear springs in the mountings, others suspect it to be a consequence of variable structural damping. More details of these phenomena can be found in the work by Toebes [4], Griffin [5], Tanida *et al.* [6], Griffin and Ramberg [7], King [8], Durgin *et al.* [9], Lecointe *et al.* [10], Chen [11], Williamson [12], Olinger and Sreenivasan [13], Ongoren and Rockwell [14, 15], Blevins [16], Mittal and Tezduyar [17], Mittal *et al.* [18], Chang and Sa [19], and Mittal and Kumar [20]. Many of these studies focus on the wake of the cylinder that is subjected to forced oscillations at various frequencies, including those that are sub- and super-harmonics of the natural vortex-shedding frequency for a stationary cylinder. Some of the studies deal with vortex-induced oscillations of a cylinder mounted on flexible supports. Most of the earlier research efforts are based on laboratory experiments while some of the more recent ones [10, 17–20] utilize computational methods.

Mittal and Tezduyar [17] reported their results for a computational study of flows past an oscillating cylinder using the finite-element method. They observed that a cylinder subjected to in-line oscillations at a certain frequency results in a symmetric mode of vortex shedding. For a cylinder restricted to cross-flow vortex-induced vibrations, they were able to observe the phenomena of lock-in and hysteresis. The Reynolds numbers for their computations are in the range of 290–300. They also attempted to explain the cause of hysteresis through numerical experiments and concluded that it is a consequence of lock-in. Lock-in occurs only if the vibration amplitude of the cylinder is greater than a certain threshold value [1]. For a certain range of Reynolds number, if the initial condition corresponds to a cylinder vibrating with large amplitude that is beyond the threshold value for lock-in, the vortex-shedding frequency locks on to the structural frequency and one realizes a high-amplitude solution. On the other hand, if one begins with a solution that corresponds to low-amplitude oscillations, that is below the threshold required for lock-in, a low-amplitude solution is realized. Later, in another study, Mittal and Kumar [20] applied their methodology to investigate the fluid-induced vibrations of a lighter cylinder, mounted on lightly damped spring supports, and free to move in cross-flow and in-line directions. The mass of the oscillator in this study is 1/100th of the one in the earlier investigation by Mittal and Tezduyar [17]. The lighter mass is used to encourage in-line oscillations. The Reynolds number for their study is 325 and computations are carried out for various values of the structural frequency including the sub- and super-harmonics of the natural vortex-shedding frequency for a stationary cylinder. The computations lead to various interesting observations. Lock-in is observed for a range of values of the structural frequency, but, in a slightly modified form. Over a certain range of structural frequency (F_s), when it is slightly larger than the natural vortex-shedding frequency (F_o), the vortex-shedding frequency of the oscillating cylinder does not exactly match the structural frequency; there is a slight *detuning* that increases as F_s moves away from F_o. Mittal and Kumar referred to it as *soft lock-in*. They also observed that this phenomenon of soft lock-in is associated with light cylinders only. As the mass of the cylinder is increased, the vortex-shedding frequency of the oscillating cylinder shifts towards the structural frequency of the oscillator. They proposed that soft lock-in is a mechanism of the non-linear oscillator to self-limit its vibration amplitude. The flow field changes significantly to restrict the amplitude of cylinder vibration. The other mechanisms of the oscillator to restrict its vibration amplitude, via a change in the flow field, are a reduction in the magnitude of aerodynamic forces and the appearance of additional frequencies in their power spectra.

In this article, the investigation carried out by Mittal and Kumar [20] is being extended to flows at higher Reynolds numbers. The Reynolds numbers, based on the diameter of the cylinder, free-stream speed and the fluid viscosity, lie between 10^3 and 10^4. Unlike the flows for low Reynolds numbers the wake behind the cylinder, for high Reynolds numbers, is quite disorganized. In certain cases a competition is observed between various modes of vortex shedding. In this context, the dependence of the solution on the Reynolds number is observed to be quite significant. For certain cases, the effect of the mass of the oscillator is also studied.

The outline of the rest of the article is as follows. A brief review of the governing equations for incompressible fluid flow and for the motion of a rigid body under the influence of unsteady fluid forces is given in section 2. Section 3 describes the stabilized finite-element formulation of the governing equations. It is based on the space–time finite-element method in which the finite-element interpolation functions depend both on space and time. This way the deformation of the spatial domain is taken into account automatically. This method, known as the DSD/SST (deforming spatial domain/stabilized space–time) technique, was introduced by Tezduyar *et al.* [21, 22]. To stabilize the computations against spurious numerical oscillations and to enable the use of equal-order-interpolation velocity–pressure elements the Galerkin/least-squares (GLS) stabilization technique is employed. Section 3 describes the finite element formulation incorporating these stabilizing terms. To accommodate the motion of the cylinder, and therefore the mesh, special mesh-moving schemes, as described by Mittal and Tezduyar [17], are used. Such special purpose mesh-moving strategies are very quick and allow one to completely do away with the remeshing. The non-linear equation systems resulting from the finite-element discretization of the flow equations are solved using the generalized minimal residual (*GMRES*) technique [23] in conjunction with diagonal preconditioners. Results and discussions are presented in section 4 and we end with some concluding remarks in section 5.

2. THE GOVERNING EQUATIONS

Let $\Omega_t \subset \mathbb{R}^{n_{sd}}$ and $(0, T)$ be the spatial and temporal domains, respectively, where n_{sd} is the number of space dimensions, and let Γ_t denote the boundary of Ω_t. The spatial and temporal co-ordinates are denoted by $\mathbf{x}$ and t. The Navier–Stokes equations governing incompressible fluid flow are

$$\rho\left(\frac{\partial \mathbf{u}}{\partial t} + \mathbf{u}\cdot\nabla\mathbf{u} - \mathbf{f}\right) - \nabla\cdot\boldsymbol{\sigma} = 0 \quad \text{on } \Omega_t \text{ for } (0, T), \tag{1}$$

$$\nabla\cdot\mathbf{u} = 0 \quad \text{on } \Omega_t \text{ for } (0, T). \tag{2}$$

Here ρ, $\mathbf{u}$, $\mathbf{f}$ and $\boldsymbol{\sigma}$ are the density, velocity, body force and the stress tensor respectively. The stress tensor is written as the sum of its isotropic and deviatoric parts:

$$\boldsymbol{\sigma} = -p\mathbf{I} + \mathbf{T}, \quad \mathbf{T} = 2\mu\boldsymbol{\varepsilon}(\mathbf{u}), \quad \boldsymbol{\varepsilon}(\mathbf{u}) = \tfrac{1}{2}((\nabla\mathbf{u}) + (\nabla\mathbf{u})^{\mathrm{T}}), \tag{3}$$

where p and μ are the pressure and viscosity. Both the Dirichlet and Neumann-type boundary conditions are accounted for, represented as

$$\mathbf{u} = \mathbf{g} \quad \text{on } (\Gamma_t)_g, \qquad \mathbf{n}\cdot\boldsymbol{\sigma} = \mathbf{h} \quad \text{on } (\Gamma_t)_h, \tag{4}$$

where $(\Gamma_t)_g$ and $(\Gamma_t)_h$ are complementary subsets of the boundary Γ_t. The initial condition on the velocity is specified on Ω_t at $t = 0$:

$$\mathbf{u}(\mathbf{x}, 0) = \mathbf{u}_0 \quad \text{on } \Omega_0, \tag{5}$$

where $\mathbf{u}_0$ is divergence free.

A solid body immersed in the fluid experiences unsteady forces and in certain cases may exhibit rigid body motion. The motion of the body, in the two directions along the cartesian axes, is governed by the following equations:

$$\ddot{X} + 2\pi F_s \zeta \dot{X} + (\pi F_s)^2 X = \frac{C_D}{M} \quad \text{for } (0, T), \tag{6}$$

$$\ddot{Y} + 2\pi F_s \zeta \dot{Y} + (\pi F_s)^2 Y = \frac{C_L}{M} \quad \text{for } (0, T). \tag{7}$$

Here, F_s is the reduced natural frequency of the oscillator, ζ is the structural damping coefficient, M is the non-dimensional mass of the body, while C_L and C_D are the instantaneous lift and drag coefficients for the body respectively. The free-stream flow is assumed to be along the x-axis, $\ddot{X}$, $\dot{X}$ and X denote the normalized in-line acceleration, velocity and displacement of the body, respectively, while $\ddot{Y}$, $\dot{Y}$ and Y represent the same quantities associated with the cross-flow motion. In the present study, in which the rigid body is a circular cylinder, the displacement and velocity are normalized by the radius of the cylinder and the free-stream speed respectively. The reduced natural frequency of the system, F_s is defined as $2f_s a/U_\infty$, where f_s is the actual frequency of the oscillator, a is the radius of the cylinder and U_∞ is the free-stream speed of the flow. The non-dimensional mass of the cylinder is defined as $M = 2m_b/\rho_\infty a^2$, where m_b is the actual mass of the oscillator and ρ_∞ is the density of the fluid. The initial conditions for the displacement and velocity of the cylinder are specified at $t = 0$:

$$X(0) = X_0, \quad \dot{X}(0) = \dot{X}_0, \tag{8}$$

$$Y(0) = Y_0, \quad \dot{Y}(0) = \dot{Y}_0. \tag{9}$$

The equations governing the fluid flow are solved in conjunction with those for the motion of the cylinder. The force acting on the body is calculated by integrating the flow variables on the body surface. The resulting drag and lift coefficients are used to compute the displacement and velocity of the body which are then used to update the location of the body and the no-slip boundary condition for the velocity field on the body surface.

3. FINITE-ELEMENT FORMULATIONS

To accommodate the motion of the cylinder and the deformation of the mesh the stabilized finite-element formulation is employed. In order to construct the finite-element function spaces for the space–time method, we partition the time interval $(0, T)$ into subintervals $I_n = (t_n, t_{n+1})$, where t_n and t_{n+1} belong to an ordered series of time levels $0 = t_0 < t_1 < \cdots < t_N = T$. Let $\Omega_n = \Omega_{t_n}$ and $\Gamma_n = \Gamma_{t_n}$. We define the space–time slab Q_n as the domain enclosed by the surfaces, Ω_n, Ω_{n+1}, and P_n, where P_n is the surface described by the boundary Γ_t as t traverses I_n. As is the case with Γ_t, surface P_n is decomposed into $(P_n)_g$ and $(P_n)_h$ with respect to the type of boundary condition (Dirichlet or Neumann) being imposed. For each space–time slab we define the corresponding finite-element function

spaces $(\mathscr{S}_{\mathbf{u}}^h)_n$, $(\mathscr{V}_{\mathbf{u}}^h)_n$, $(\mathscr{S}_p^h)_n$, and $(\mathscr{V}_p^h)_n$. Over the element domain, this space is formed by using first order polynomials in space and time. Globally, the interpolation functions are continuous in space but discontinuous in time.

The stabilized space–time formulation for deforming domains is then written as follows: given $(\mathbf{u}^h)_{n-}$, find $\mathbf{u}^h \in (\mathscr{S}_{\mathbf{u}}^h)_n$ and $p^h \in (\mathscr{S}_p^h)_n$ such that $\forall \mathbf{w}^h \in (\mathscr{V}_{\mathbf{u}}^h)_n$, $q^h \in (\mathscr{V}_p^h)_n$

$$\int_{Q_n} \mathbf{w}^h \cdot \rho\left(\frac{\partial \mathbf{u}^h}{\partial t} + \mathbf{u}^h \cdot \nabla \mathbf{u}^h - \mathbf{f}\right) dQ + \int_{Q_n} \boldsymbol{\varepsilon}(\mathbf{w}^h) : \boldsymbol{\sigma}(p^h, \mathbf{u}^h)\, dQ + \int_{Q_n} q^h \nabla \cdot \mathbf{u}^h\, dQ$$

$$+ \sum_{e=1}^{n_{el}} \int_{Q_n^e} \frac{1}{\rho} \tau \left[\rho\left(\frac{\partial \mathbf{w}^h}{\partial t} + \mathbf{u}^h \cdot \nabla \mathbf{w}^h\right) - \nabla \cdot \boldsymbol{\sigma}(q^h, \mathbf{w}^h)\right]$$

$$\cdot \left[\rho\left(\frac{\partial \mathbf{u}^h}{\partial t} + \mathbf{u}^h \cdot \nabla \mathbf{u}^h - \mathbf{f}\right) - \nabla \cdot \boldsymbol{\sigma}(p^h, \mathbf{u}^h)\right] dQ$$

$$+ \sum_{e=1}^{n_{el}} \int_{Q_n^e} \delta \nabla \cdot \mathbf{w}^h \rho \nabla \cdot \mathbf{u}^h\, dQ + \int_{\Omega_n} (\mathbf{w}^h)_n^+ \cdot \rho((\mathbf{u}^h)_n^+ - (\mathbf{u}^h)_n^-)\, d\Omega = \int_{(P_n)_h} \mathbf{w}^h \cdot \mathbf{h}^h\, dP. \quad (10)$$

This process is applied sequentially to all the space–time slabs $Q_1, Q_2, \ldots, Q_{N-1}$. In the variational formulation given by equation (10), the following notation is used:

$$(\mathbf{u}^h)_n^{\pm} = \lim_{\varepsilon \to 0} \mathbf{u}(t_n \pm \varepsilon), \quad (11)$$

$$\int_{Q_n} (\cdots)\, dQ = \int_{I_n} \int_{\Omega_n} (\cdots)\, d\Omega\, dt, \quad (12)$$

$$\int_{P_n} (\cdots)\, dP = \int_{I_n} \int_{\Gamma_n} (\cdots)\, d\Gamma\, dt. \quad (13)$$

The computations start with

$$(\mathbf{u}^h)_0^- = \mathbf{u}_0, \quad (14)$$

where $\mathbf{u}_0$ is divergence free.

In the variational formulation given by equation (10), the first three terms and the right-hand side constitute the Galerkin formulation of the problem. The series of element-level integrals involving the coefficients τ and δ are the least-squares terms that are added to the basic Galerkin formulation to ensure the stability of the computations. This type of stabilization is referred to as the Galerkin/least-squares (GLS) procedure and is a generalization of the streamline-upwind/Petrov–Galerkin (SUPG) and pressure-stabilizing/Petrov–Galerkin) (PSPG) method [24]. In the current formulation τ and δ are given as

$$\tau = \left(\left(\frac{2\|\mathbf{u}^h\|}{h}\right)^2 + \left(\frac{4\nu}{h^2}\right)^2\right)^{-1/2}, \quad (15)$$

$$\delta = \frac{h}{2}\|\mathbf{u}^h\| z, \quad (16)$$

where

$$z = \begin{cases} \left(\frac{\mathrm{Re}_u}{3}\right), & \mathrm{Re}_u \leqslant 3, \\ 1, & \mathrm{Re}_u > 3 \end{cases}$$

and Re_u is the cell Reynolds number. Both stabilization terms are weighted residuals, and therefore maintain the consistency of the formulation. The sixth term in equation (10) enforces weak continuity of the velocity field across the space–time slabs.

The equations of motion for the oscillator given by equations (6)–(9) are also cast in the space–time formulation in the same manner as described in the work by Tezduyar *et al.* [22] and Mittal [25].

4. RESULTS AND DISCUSSIONS

A cylinder of non-dimensional mass $M = 4{\cdot}7273$ and the structural damping coefficient $\zeta = 3{\cdot}3 \times 10^{-04}$ is placed in a uniform flow. The outer boundary of the computational domain is rectangle whose upstream and downstream edges are located at 8 and 22·5 cylinder diameters from the center of the cylinder respectively. The upper and lower edges are placed at eight diameters from the center of the cylinder. At the cylinder surface, the no-slip boundary condition is applied for the velocity. Free-stream values are assigned for the velocity at the upstream boundary while at the downstream boundary, the viscous stress vector is assumed to be zero. On the upper and lower boundaries, the component of velocity normal to and the component of stress vector along these boundaries is prescribed zero value. Computations are carried out for Reynolds numbers 1000, 1500 and 10000 for various values of the non-dimensional structural frequency (F_s) of the spring–mass system. The effect of mass (M) of the oscillator is also investigated for some cases. The Reynolds number is based on the diameter of the cylinder, free-stream velocity and the viscosity of the fluid. Results for a similar set-up at Reynolds number 325 have been reported in an earlier article [20]. Mittal and Tezduyar [17] reported results for a heavier cylinder whose motion is restricted to the cross-flow direction for flows with Reynolds numbers in the range of 290–360. The mass of the cylinder in the present study and the one reported in reference [20] is 1/100th of the one considered by Mittal and Tezduyar [17]. The lower mass of the oscillator is to encourage in-line oscillations. The damping coefficient has the same value in all the three studies.

All the computations reported in this article are carried out on the Digital workstations at IIT Kanpur in 64 bit precision. Equal-in-order basis functions for velocity and pressure, that are bilinear in space and linear in time, are used and $2 \times 2 \times 2$ Gaussian quadrature is employed for numerical integration. The non-linear equation systems resulting from the finite-element discretization of the flow equations are solved using the GMRES technique [23] in conjunction with diagonal preconditioners.

In all the cases, first the fully developed unsteady solution is computed for flow past a stationary cylinder at the Reynolds number of interest. This solution is used as an initial condition for computing the flow past the oscillating cylinder. The computations are carried out using three finite-element meshes. Mesh M1 consists of 6181 nodes and 6000 elements, M2 has 8453 nodes and 8230 elements while the finest mesh the mesh M3 is made up of 8537 nodes and 8330 elements. A view of the mesh, M3, and its close-up is shown in Figure 1. The mesh-moving scheme is the same as the one used by Mittal and Tezduyar [17]. Figure 2 summarizes the variation of the non-dimensional cross-flow and in-line oscillation amplitudes, and the vortex-shedding frequency with respect to the structural frequency of

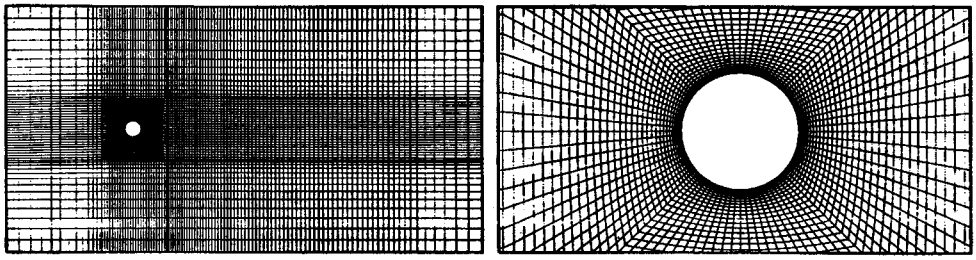

Figure 1. Flow past an oscillating cylinder: the finite-element mesh, M3, with 8537 nodes and 8330 elements.

the oscillator for various Reynolds numbers. The Strouhal number corresponding to the vortex-shedding frequency for the stationary cylinder for all the three Reynolds numbers, from our computations, is 0·25. This value will be referred to as the natural vortex-shedding frequency (F_o) in the rest of the article. Compared to the experimental results [26] this value is slightly on the higher side. It has been observed in the past by various researchers [27–29] that 2-D computations tend to over-predict the mean drag coefficient and the Strouhal number while results from 3-D computations are closer to experimental observations. It is also well known that beyond a Reynolds number of approximately 300 the 3-D effects in the wake of the cylinder become significant [30]. The Reynolds number for the flows considered in this article is much higher than this critical value and 3-D effects are expected to be important. However, due to the constraints of the available computational resources, simulations reported in this article are restricted to 2-D only. The 3-D effects will be taken up in a later study.

From Figure 2 it can be observed that the effect of the Reynolds number on the vortex-shedding frequency of the oscillating cylinder is significant when the structural frequency (F_s) of the oscillator is close to the natural shedding frequency (F_o) of the cylinder. On the other hand, when the value of F_s is relatively far off from F_o the effect of Reynolds number on the vortex-shedding frequency is not too large. In general, the amplitude of vibrations in the cross-flow direction is larger compared to that in the in-line direction. It is well known that the motion of the cylinder alters the flow field significantly. For a cylinder that is forced to vibrate at a frequency that is slightly different from the natural vortex-shedding frequency (F_o), and an amplitude that is larger than a certain threshold value, the phenomenon of lock-in is observed; the vortex-shedding frequency locks on to the vibration frequency. A similar phenomenon is observed in the case of vortex-induced oscillations of a cylinder mounted on spring support. Mittal and Tezduyar [17] reported their computational results for a cylinder that is allowed to vibrate in the cross-flow direction only. They observed lock-in and hysteresis and were able to explain it based on data from experiments of other researchers. Mittal and Kumar [20] carried out an investigation for a lighter cylinder that is free to vibrate in cross-flow and in-line directions. They observed that the lock-in frequency depends on the mass of the oscillator. For light cylinders, over a certain range of structural frequency, when F_s is slightly larger than F_o the vortex-shedding frequency of the oscillating cylinder does not exactly match the structural frequency; there is a slight *de-tuning* that increases as F_s moves away from F_o. They termed the phenomenon as soft lock-in and suggested that this is a mechanism of the non-linear oscillator to self-limit its oscillation amplitudes. Both the above-mentioned computational studies were carried out for flows with Reynolds numbers in the vicinity of 325. In the present study it is observed, as before, that the flow is significantly altered as a result of the cylinder motion.

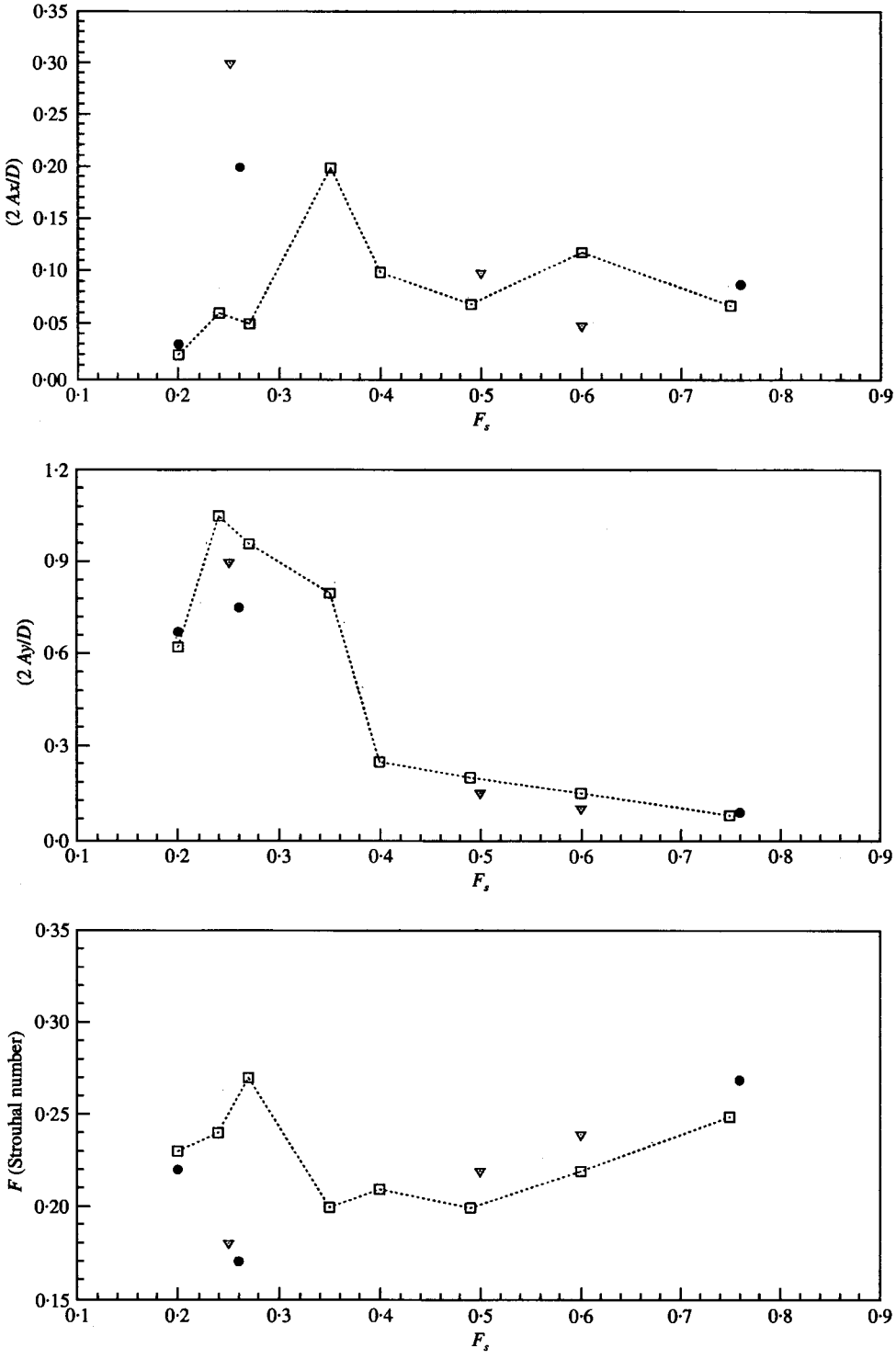

Figure 2. Flow past an oscillating cylinder: variation of the non-dimensional in-line and cross-flow oscillation amplitudes, and the Strouhal number (related to the dominant frequency in the time history of the lift coefficient) with respect to the structural frequency of the oscillator. ···⊡···, Re = 1000; ●, Re = 1500; ▽, Re = 10 000.

The "de-tuning" that was observed for the Reynolds number 325 flow is seen in a more exaggerated form in the present case.

4.1. Re = 1000

The solution for flow past a stationary cylinder at Reynolds number 1000 is shown in the top rows of Figures 3 and 4. We observe that the Strouhal number corresponding to the dominant frequency of the lift variation is 0·25 and the mean drag coefficient is 1·48. The amplitude of the unsteady component of drag coefficient is 0·21, while that of the lift coefficient is 1·36. During each cycle of vortex shedding a vortex is alternately shed from the upper and lower surfaces of the cylinder. They convect downstream to form the karman vortex street as shown in Figure 3.

The first case of the vortex-induced oscillation in this study corresponds to the non-dimensional structural frequency (F_s) of 0·20. The time histories of the drag and lift coefficients in this case are shown in Figure 4. The trajectory of the cylinder is shown in Figure 5. It can be observed that the cylinder vibrations are mainly in the cross-flow direction. As soon as the cylinder is released from rest the in-line oscillations are quite significant but eventually they get damped out. The vortex shedding frequency for the oscillating cylinder is 0·23. This value of the vortex-shedding frequency corresponds to neither F_s nor F_o; it lies somewhere in between. As was observed in an earlier study by Mittal and Kumar [20] for lower Reynolds number, this is a soft lock-in. Figure 3 shows the vorticity and pressure fields for the temporally periodic solution. Compared to the flow for a stationary cylinder, it can be observed that as a result of the cylinder vibrations the lateral width of the wake increases and longitudinal spacing between the vortices decreases. The latter effect can be attributed to the decrease in the vortex-shedding frequency of the oscillating cylinder. For $F_s = 0{\cdot}24$, compared to the previous case, the amplitude of the in-line and cross-flow oscillations is larger for this value of F_s. The vortex-shedding frequency is 0·24. The frequency of the cross-flow oscillations is equal to the structural frequency of the oscillator. As expected, since the drag force experienced by the cylinder oscillates at twice the frequency of the lift force, the in-line vibrations occur at twice the cross-flow oscillation frequency of the oscillator. The trajectory of the cylinder corresponds to a *Lissajou* figure of *8*. The same observations have been made earlier by researchers during laboratory experiments [11, 16]. A very similar behavior is exhibited by the oscillator for $F_s = 0{\cdot}27$. Lock-in is observed in this case also. The vortex-shedding frequency of the oscillating cylinder locks-in to the structural frequency. It is interesting to observe that, as in the previous case, the power spectrum of the lift coefficient displays two peaks (F_s and $3F_s$), while the drag coefficient oscillates with only one frequency ($2F_s$). This is perhaps related to the self-limiting nature of the motion of the non-linear oscillator. It is well known that the vortex-excited oscillations of a bluff body are self-limited; the fluid flow adjusts so that the oscillation amplitude is restricted to a certain upper limit. It has been observed by Mittal and Kumar [20] that the various mechanisms by which the oscillator is able to self-limit its vibration amplitude are a reduction in the amplitude of the aerodynamic forces, appearance of additional frequency components in the time histories of the fluid forces and de-tuning of the vortex-shedding frequency from the structural frequency. The extra peak in the lift coefficient ($3F_s$), in the present case, is perhaps to limit the amplitude of cross-flow cylinder vibration. Since the in-line oscillations are of much smaller amplitude, such a peak is not seen in the power spectrum for the drag coefficient. Another interesting observation that can be made from the time histories in the simulations is regarding the abruptness with which the cylinder motion latches on to a limit cycle. For

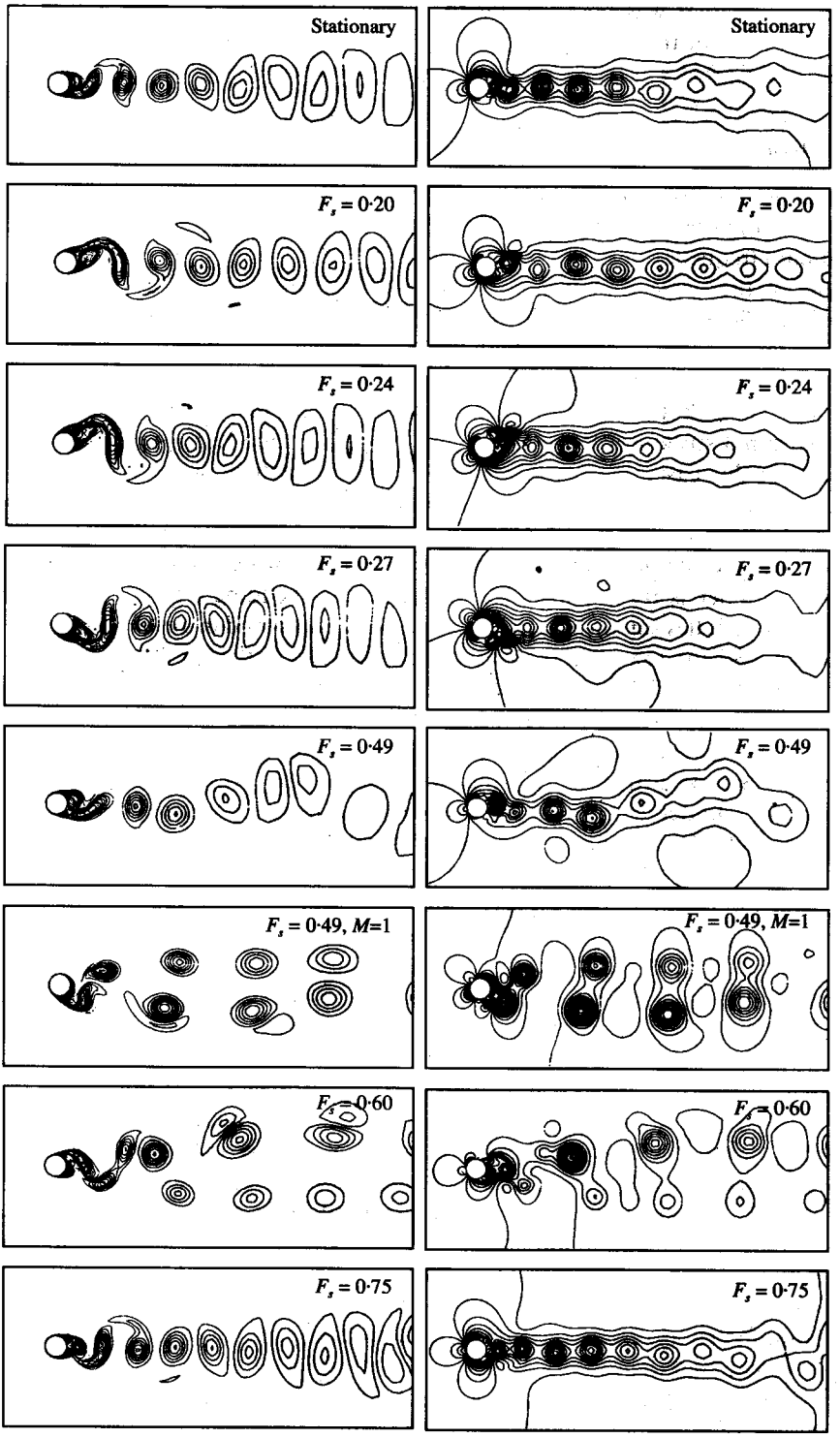

Figure 3. Re = 1000 flow past stationary and oscillating cylinder: vorticity and pressure fields for the various cases.

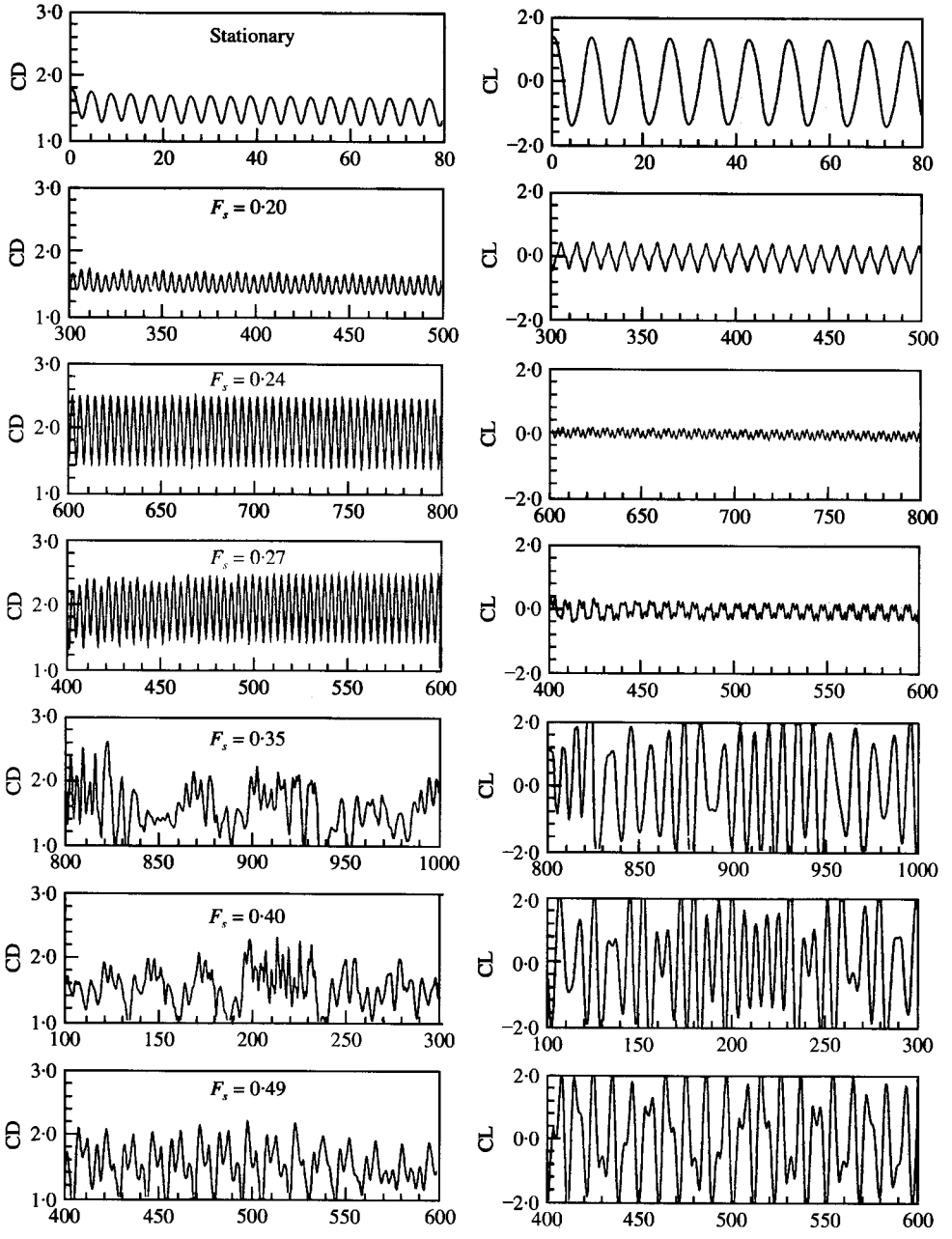

Figure 4. Re = 1000 flow past stationary and oscillating cylinder: time histories of the drag and lift coefficients for the stationary cylinder and for $F_s = 0{\cdot}20$, 0·24, 0, 27, 0·35, 0·40, and 0·49.

example, for $F_s = 0{\cdot}27$ the cylinder undergoes fairly disorganized motion till about $t = 350$. At $t = 370$, approximately, the vortex shedding becomes very regular and the cylinder motion also reaches a temporally periodic state. This highlights the need of long-time integration of the governing equations to observe the long-term dynamics of such non-linear systems. Unlike the previous cases, for $F_s = 0{\cdot}35$, the cylinder motion and the vortex

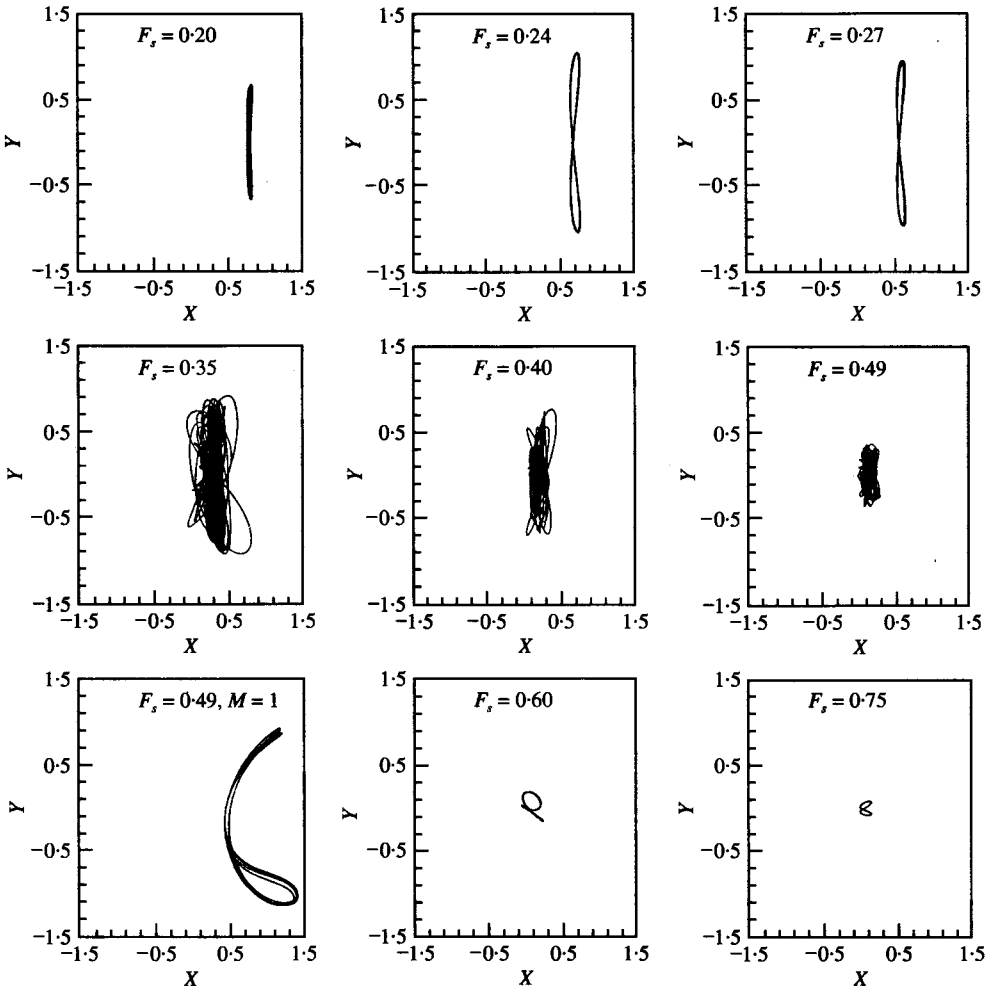

Figure 5. Re = 1000 flow past an oscillating cylinder: trajectories of the cylinder for the various cases.

shedding do not reach a temporally periodic solution in this case. The time histories suggest the possibility of mode-competition between two (or more) modes of vortex shedding. The vorticity and pressure fields at $t = 790, 820, 1060, 1160$ and 1240 are shown in Figure 6. This picture confirms the presence of competition between two modes of vortex shedding. One of the two modes is the one that is observed for a stationary cylinder in which counter-rotating vortices are shed alternately from upper and lower surfaces of the cylinder in each cycle of vortex shedding. Ongoren and Rockwell [15] refer to this mode as Antisymmetrical mode A-I. The other mode of vortex shedding that can be observed in Figure 6 is the Antisymmetrical mode A-III in which, during each cycle of shedding, in addition to a pair of counter-rotating vortices another weak vortex is shed from the cylinder. Williamson and Roshko [12] have also observed mode-competition in their laboratory experiments and have explained the cause of the sudden mode changes. The solutions for $F_s = 0{\cdot}40$ are shown in Figures 4 and 7. The flow pictures in Figure 7 are at $t = 245, 285, 290$ and 352. *Swinging* of the near wake can be observed from this figure. Such wake swings are not observed in flows at low Reynolds numbers [20]. The next computation is for $F_s = 0{\cdot}49$ $(= 2F_o)$. This

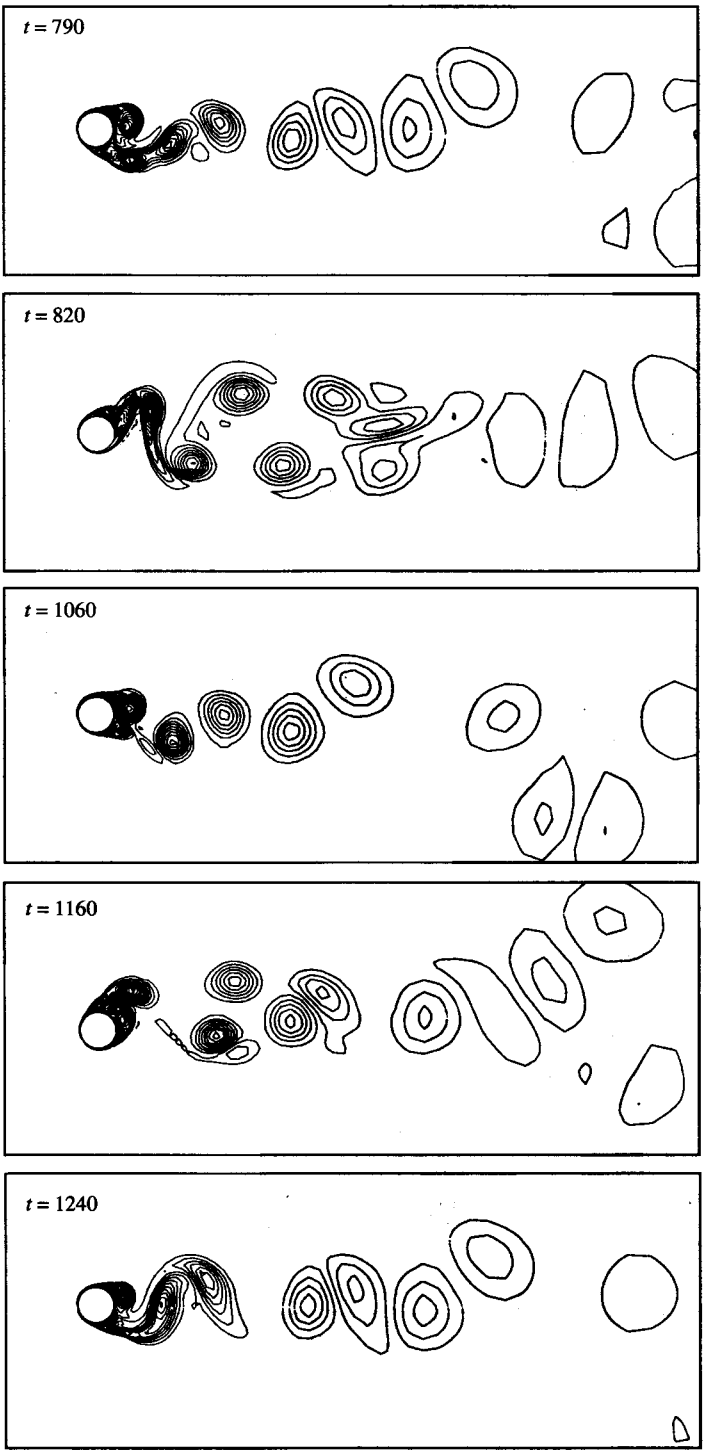

Figure 6. Re = 1000 flow past an oscillating cylinder with $F_s = 0{\cdot}35$: vorticity and pressure fields at $t = 790$, 820, 1060, 1160 and 1240.

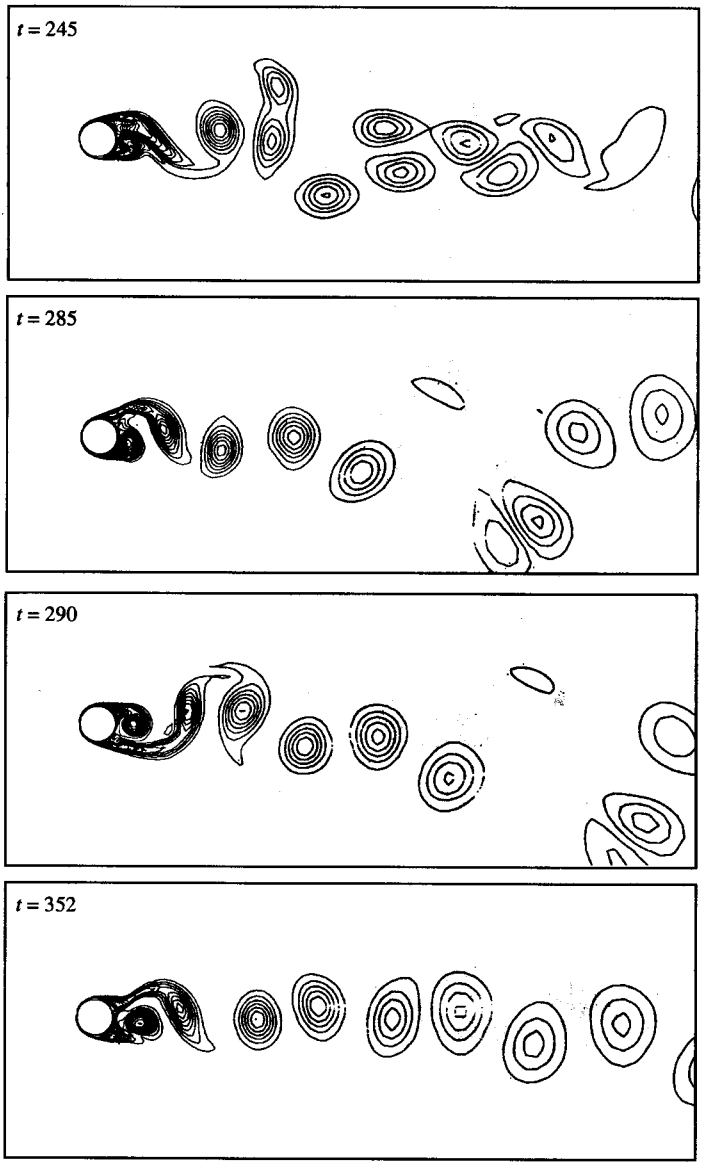

Figure 7. Re = 1000 flow past an oscillating cylinder with $F_s = 0{\cdot}40$: vorticity and pressure fields at $t = 245$, 285, 290 and 352.

case is quite interesting. From Figure 4 it can be observed that the quantities corresponding to the in-line oscillations are closer to a temporally periodic state compared to those for the cross-flow vibrations. This may be related to the observation that in this case the structural frequency coincides with the frequency of variation of drag for flow past a stationary cylinder. To further encourage the in-line oscillations of the cylinder this case is recomputed with a lower mass of the oscillator ($M = 1{\cdot}0$). The solutions for this computation are shown in Figures 8 and 3. Almost immediately after the cylinder is released from rest its motion latches on to the limit cycle. It displays a two-period mode for the in-line motion and a single-period mode for the cross-flow oscillations. The trajectory of the cylinder is quite

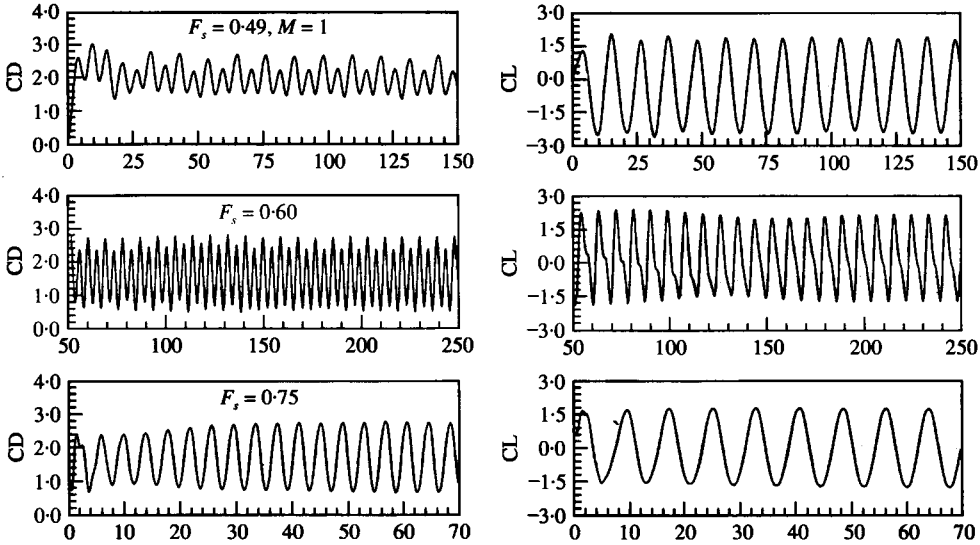

Figure 8. Re = 1000 flow past an oscillating cylinder: time histories of the drag and lift coefficients for $F_s = 0{\cdot}49$ and $M = 1$ and for $F_s = 0{\cdot}60$ and $0{\cdot}75$.

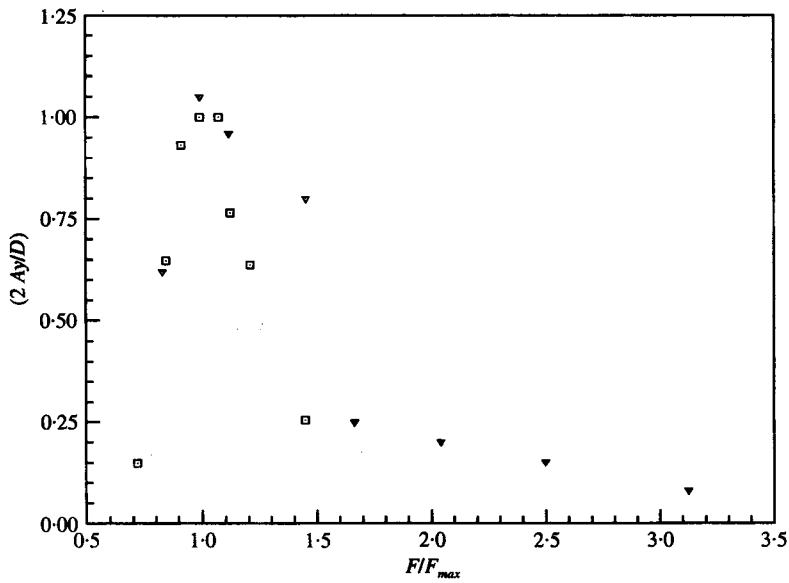

Figure 9. Re = 1000 flow past an oscillating cylinder: variation of the non-dimensional cross-flow oscillation amplitudes, with the normalized reduced structural frequency. The results from the experiments of Griffin and Ramberg are also shown. F_{max} is the reduced frequency for which the maximum oscillation amplitude is observed. ⊡, Griffin and Ramberg; ▽, Present computations.

different from that observed in the previous cases. The vortex-shedding mode corresponds to the Antisymmetrical mode A-III [15] in which during each cycle of vortex shedding a pair of counter-rotating vortices and another single weaker vortex is shed from the cylinder. The same mode of vortex shedding is observed for $F_s = 0{\cdot}60$ (with the original mass of the oscillator). The flow picture at a time instant for the temporally periodic

solution is shown in Figure 3. In the previous case ($M = 1$, $F_s = 0.49$), the additional single vortex, that is shed in addition to the vortex pair of each cycle, is released from the upper surface while in the present case ($M = 4{\cdot}7273$, $F_s = 0{\cdot}60$), it is released from the lower surface of the cylinder. The power spectrum of the lift coefficient, in the current case, shows two peaks, one at the vortex-shedding frequency (0·22) and the other at twice the value (0·44). In the other cases of periodic vortex shedding for an oscillating cylinder when the Antisymmetrical mode A-I is observed, the second peak in the power spectrum of the lift coefficient corresponds to thrice the vortex-shedding frequency. The cause of the appearance of the second peak is quite different in the two cases. For $F_s = 0{\cdot}60$ it is caused by the additional single vortex shed during each vortex-shedding cycle while the peak in the latter case is due to the local modification of the flow to self-limit the cross-flow vibration amplitude. The last case that has been studied for Re = 1000 is for $F_s = 0{\cdot}75$ ($=3F_o$). The solutions corresponding to this case are shown in Figures 3, 5 and 8. The cylinder undergoes small amplitude vibrations and the flow field is quite similar to that for a stationary cylinder. The power spectrum for the lift coefficient shows only one dominant frequency. This is consistent with our earlier observation that for the Antisymmetrical mode A-I of vortex shedding the second peak in the power spectrum for the lift coefficient appears only when the cylinder vibrates with a large amplitude in the cross-flow direction.

In Figure 9 results from the present computations are compared to the results of Griffin and Ramberg [31] for their experiments with a cylinder allowed to vibrate in water. It can be noticed that the two sets of results are in fairly good agreement. This observation increases our confidence in the present set of computations.

4.2. Re = 1500

Based on the observation that the flows at Re = 1500 and 1000 for a stationary cylinder are quite similar, it is expected that the qualitative behavior of the oscillator at the two Reynolds numbers should be the same. However, as will be seen later in this section, for certain values of F_s, qualitatively different behavior is seen for the two Reynolds numbers. Figure 10 shows the time histories of the drag and lift coefficients for the stationary cylinder at Re = 1500. It is quite similar to the corresponding solution at Re = 1000. The amplitude of the time-varying components of lift and drag coefficients are a little larger for Re = 1500 but the Strouhal number corresponding to the variation of lift coefficient is the same for both the flows. The top row in Figure 11 shows the vorticity and pressure fields at one time instant for the temporally periodic solution. The rest of the rows in this figure show solutions for the oscillating cylinder. The second row shows the flow field for $F_s = 0{\cdot}20$. As a result of the cylinder motion the lateral width of the wake increases and the vortex-shedding frequency decreases as is suggested by the increased longitudinal spacing between the vortices. The time histories for the aerodynamic coefficients and displacements of the cylinder are shown in Figure 10. The trajectory of the cylinder is shown in Figure 12. The cylinder undergoes large amplitude cross-flow vibrations and relatively low amplitude in-line oscillations. Its trajectory resembles a Lissajous figure of *8*. The Strouhal number corresponding to the vortex-shedding frequency is 0·22. As was the case for $F_s = 0{\cdot}20$, Re = 1000 the vortex-shedding frequency is larger than the structural frequency but smaller than F_s and larger than F_o. The third row in Figure 11 shows the flow field for the oscillating cylinder for $F_s = 0{\cdot}26$ at $t = 363$. The related time histories are shown in Figure 10 and the trajectory of the cylinder in Figure 12. This case is very interesting from the point of view of competition between various modes of vortex shedding. The third row in Figure 11, corresponding to $t = 363$, shows the *Symmetric mode S* of vortex shedding. However, the

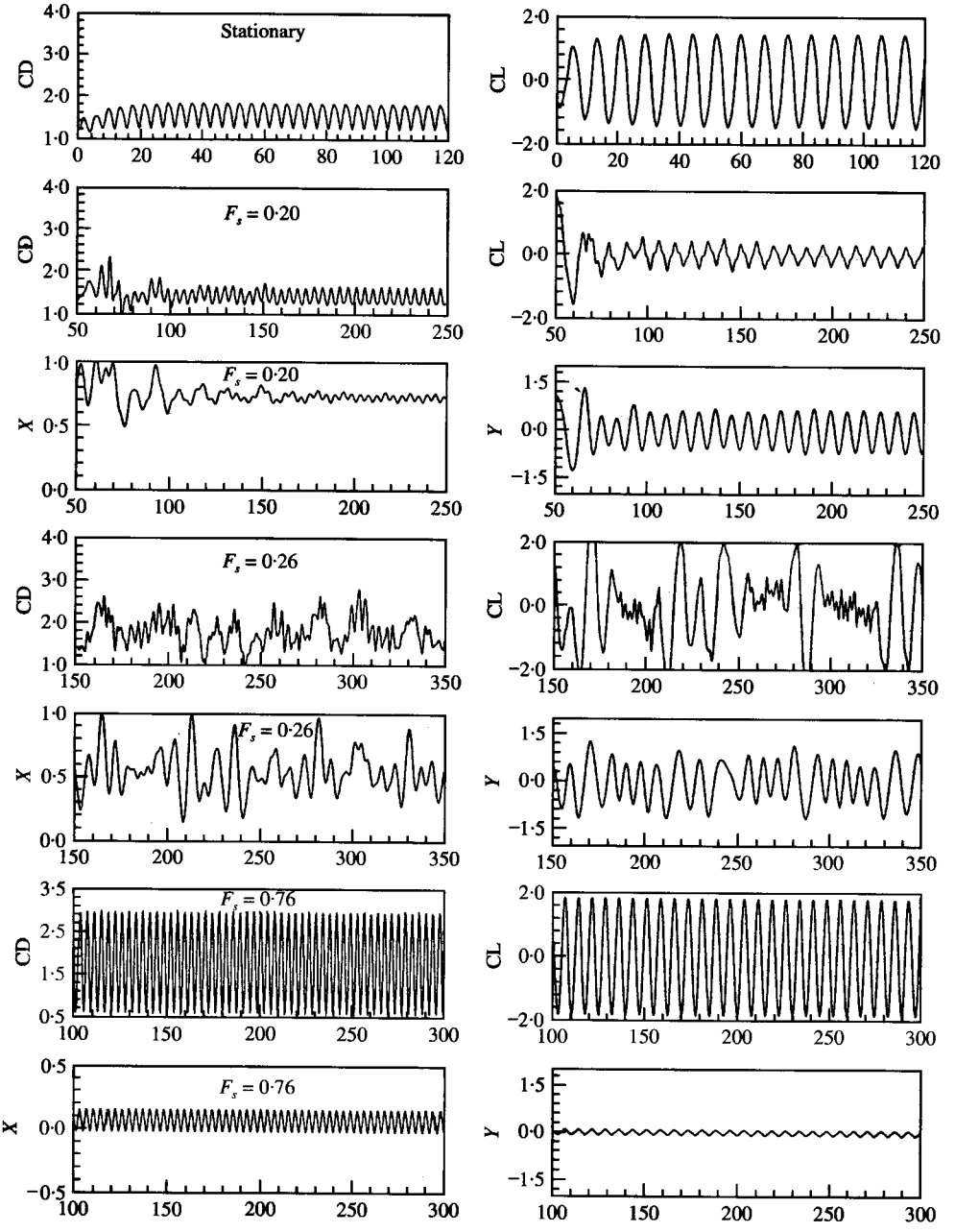

Figure 10. Re = 1500 flow past a stationary and oscillating cylinder: time histories of the drag and lift coefficients and normalized cylinder displacements.

pictures at some other time instants (not shown here) display the Antisymmetrical mode A-III of vortex shedding. This can also be observed from the time histories of the lift coefficient and cross-flow displacement of the cylinder in Figure 10. For example, for $320 < t < 350$ (anti-symmetric shedding), approximately, the amplitude of the temporal variation of lift coefficient is quite large compared to that for $300 < t < 320$ and $t > 350$ (symmetric shedding). Similarly, the cross-flow oscillations during $300 < t < 320$ and

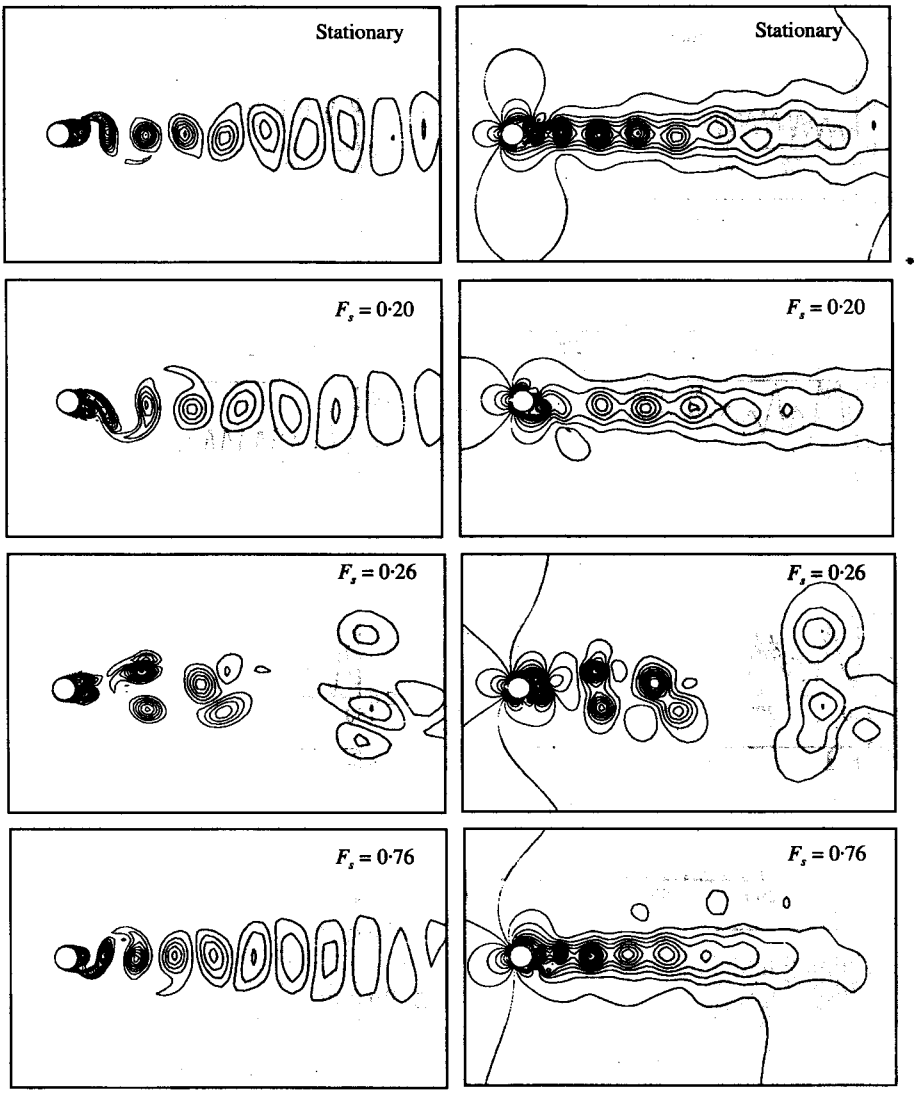

Figure 11. Re = 1500 flow past stationary and oscillating cylinder: vorticity and pressure fields for the various cases.

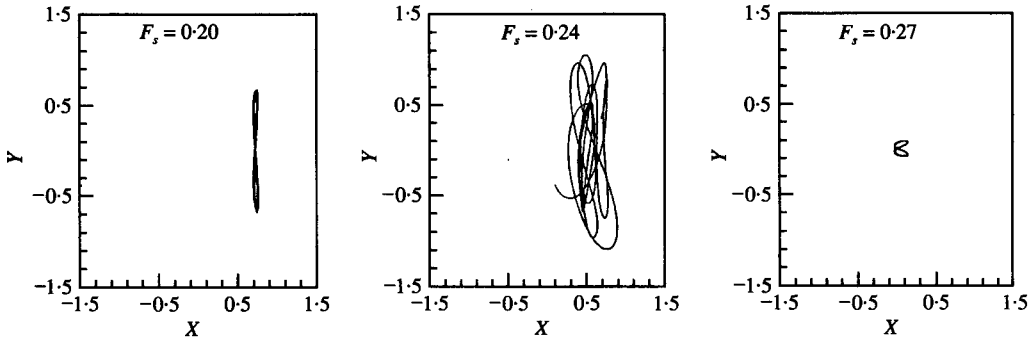

Figure 12. Re = 1500 flow past an oscillating cylinder: trajectories of the cylinder for the various cases.

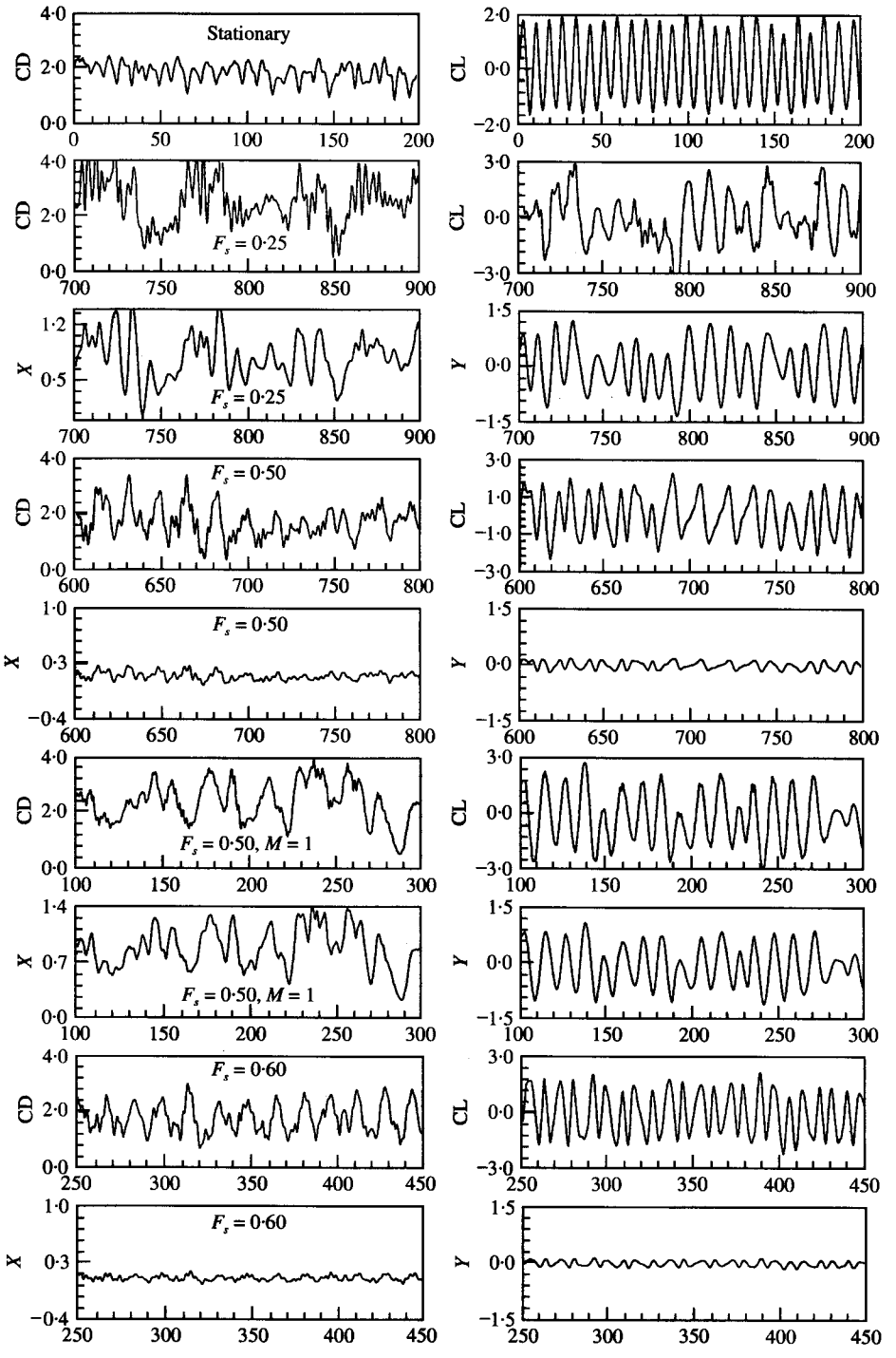

Figure 13. Re = 10^4 flow past a stationary and oscillating cylinder: time histories of the drag and lift coefficients and normalized cylinder displacements.

$t > 350$ (symmetric shedding) are smaller than those during $320 < t < 350$ (anti-symmetric shedding). Interestingly, the flow does not display such a mode competition for this value of F_s for Re = 1000. This suggests a strong dependence of the flow on Reynolds number for this range of values of F_s. The solution corresponding to $F_s = 0{\cdot}76$ $(= 3F_o)$ is shown in Figure 10 and the last row of Figure 11. The flow field looks quite similar to the flow past a stationary cylinder. The oscillation amplitudes are quite small and the path of the cylinder motion resembles a figure of *8* with comparable amplitudes of the cross-flow and in-line vibrations.

4.3. Re = 10,000

Flows past stationary cylinder at Re = 1000 and 1500 are associated with periodic vortex shedding. At larger Reynolds number the flow becomes more complex: the wake ceases to exhibit a temporally periodic nature and is accompanied by a *bias* towards a particular side, away from the center line [32]. The top row of Figure 13 shows the time histories of the drag and lift coefficients for a stationary cylinder places in a uniform flow at $\mathrm{Re} = 10^4$. The flow field at $t = 200$ is shown in Figure 14. The initial condition for this computation is the unsteady solution at $\mathrm{Re} = 10^3$. The downward bias of the wake and interesting vortex dynamics can be clearly observed from the figure. Vortex pairing and their tumbling around as they are convected downstream is quite apparent. The near wake of the cylinder suggests that the vortex shedding still corresponds to the Antisymmetrical mode A-I. In addition to the large vortex pair several smaller vortices are also shed during each cycle of vortex shedding. These smaller vortices are responsible for the additional frequencies in the power spectra for the drag coefficient. The Strouhal number based on the dominant frequency in the time histories of the drag and lift coefficient is 0·25.

The solution for the case with oscillating cylinder for $F_s = 0{\cdot}25$ $(= F_o)$ is shown in Figures 13 and 14. The trajectory of the cylinder is shown in Figure 15. It can be observed that the cylinder undergoes fairly large amplitude disorganized motion. For the stationary cylinder, it was observed that the wake behind the cylinder is biased to one side. In the present case *swinging* of wake to either side can be observed. Some of the frames during the simulation suggest the Antisymmetrical mode A-III of vortex shedding. Figures 13 and 14 also show the solution for $F_s = 0{\cdot}50$ $(= 2F_o)$. Even though the amplitudes of the unsteady components of the lift and drag coefficients is quite high, the amplitude of the cylinder oscillations is quite small. It is interesting to observe that the non-dimensional dominant frequency in the time variation of the drag coefficient and the in-line oscillations is 0·12 while that corresponding to lift coefficient and cross-flow oscillations is 0·22. Swinging of the wake and jumps between modes of vortex shedding has been observed during the simulation. For example, the flow at $t = 810$ and $t = 860$ correspond to Antisymmetrical mode A-I and Symmetrical mode S of vortex shedding respectively. To encourage larger amplitude oscillations of the cylinder the computations were also carried out with a lower mass of the oscillator ($M = 1$). The solutions for this case are shown in Figures 13 and 14. In this case the movement of the separation point on the cylinder surface is quite violent as a result of the large amplitude cylinder motion. A large number of smaller vortices are shed in addition to the ones associated with shedding for a stationary cylinder. Complex vortex interactions can be noticed in the resulting wake. The cylinder oscillations in the cross-flow direction are more organized than those in the in-line direction. Finally, results are shown for $F_s = 0{\cdot}60$ with the original mass of the oscillator ($M = 4{\cdot}7273$) in Figures 13, 14 and 15. The vortex-shedding mode for this computation suggests the usual Antisymmetrical mode A-I.

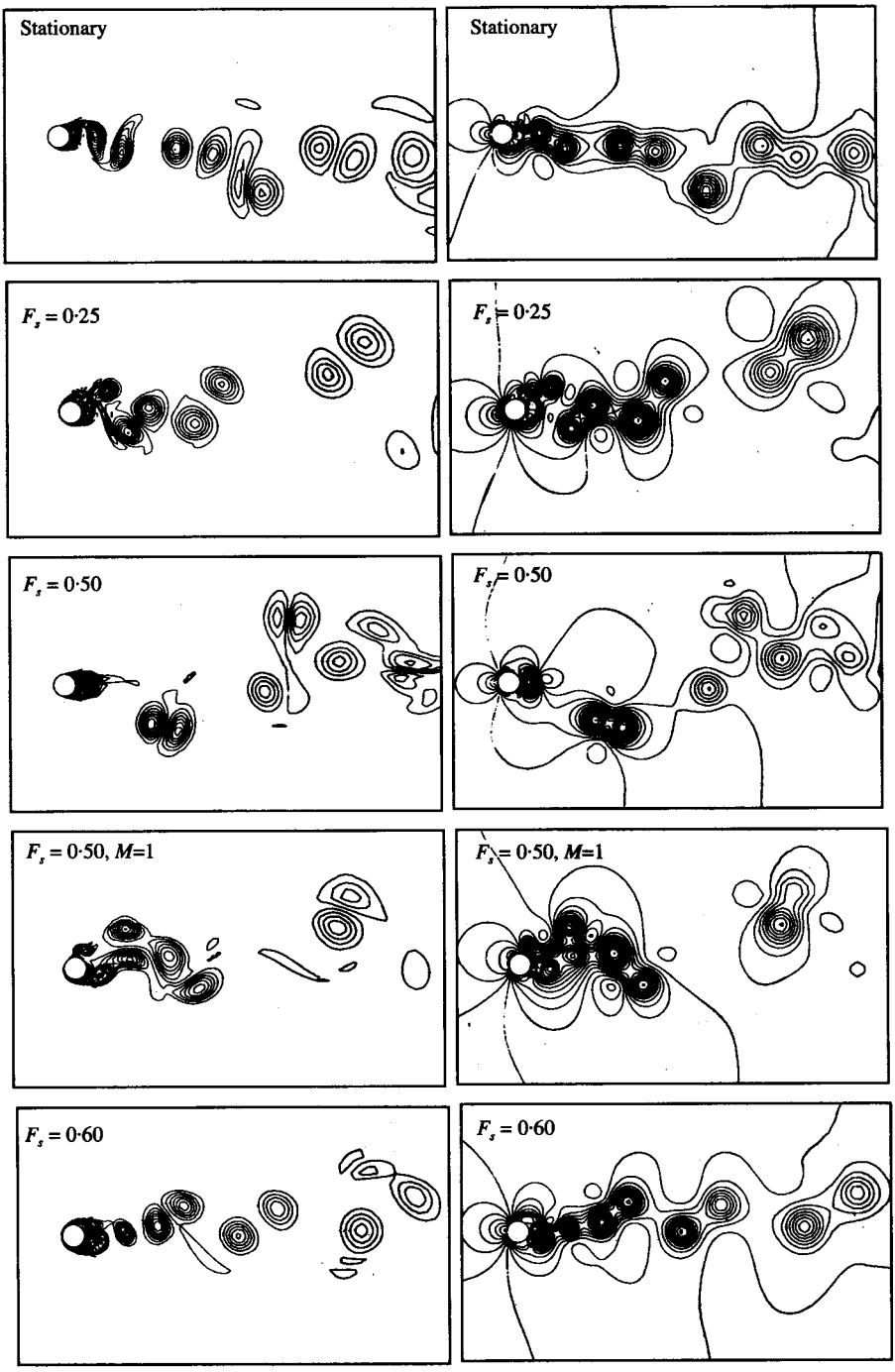

Figure 14. Re = 10^4 flow past stationary and oscillating cylinder: vorticity and pressure fields for the various cases.

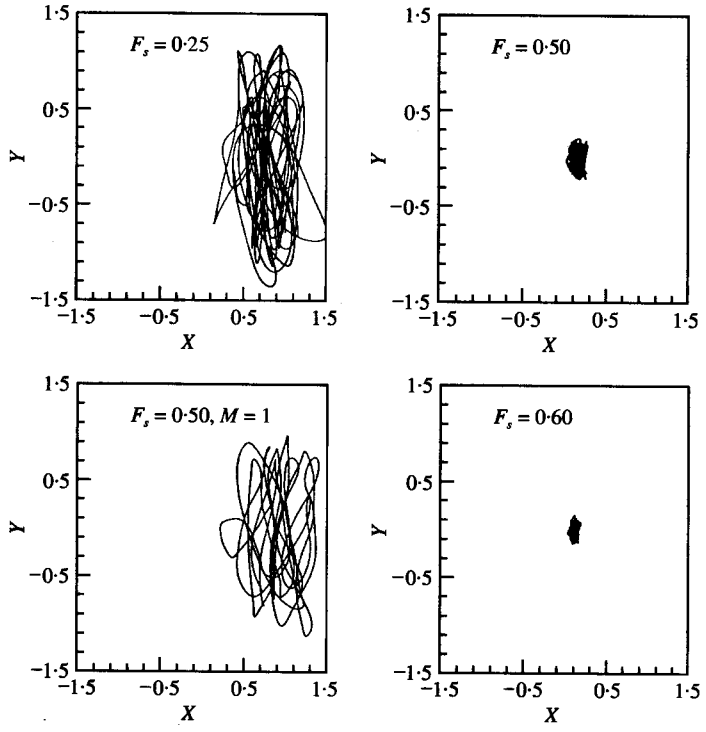

Figure 15. Re = 10^4 flow past an oscillating cylinder: trajectories of the cylinder for the various cases.

The non-dimensional frequency for the variation of drag coefficient is 0·12 while that for the lift coefficient is 0·24.

5. CONCLUDING REMARKS

Vortex-induced vibrations of a light cylinder placed in a uniform flow at Reynolds Number in the range of 10^3–10^4 have been studied using a stabilized space–time finite-element formulation. The cylinder, mounted on flexible supports, is allowed to vibrate, both in the in-line and cross-flow directions. The behavior of the oscillator for various values of the structural frequency (F_s) including those that are super-harmonics of the vortex-shedding frequency for the stationary cylinder (F_o) have been presented. The effect of the mass of the cylinder for certain cases has also been studied. Flows at lower Reynolds numbers are associated with organized wakes and the motion of the cylinder, at least at frequencies close to F_o, attains a limit cycle. The motion of the cylinder alters the fluid flow significantly. For a certain range of the structural frequency, (F_s), lock-in is observed; the vortex-shedding frequency of the oscillating cylinder shifts to F_s. In some other cases the vortex-shedding frequency of the oscillating cylinder does not exactly match the structural frequency; there is a slight *de-tuning*. This phenomenon is referred to as soft lock-in. At certain values of F_s, the motion of the cylinder affects not only the frequency of vortex shedding but also the mode of vortex shedding. In many cases, the non-linear fluid-oscillator system takes a long time to evolve from the initial condition (unsteady flow past stationary cylinder) to the final temporally periodic solution. Usually, the changeover from the long transience to the limit cycle is quite abrupt. This points to the need of accurate

long-time integration of the governing equations to study the dynamics of such non-linear systems. At higher Reynolds numbers, the vortex shedding is quite disorganized and the cylinder does not reach a temporally periodic solution. The vortex dynamics in the wake is extremely complex and so is its effect on the motion of the cylinder. High Reynolds number flows, past stationary cylinders, are associated with wakes with a *bias*; the entire wake is deflected to one side, away from the center line. For oscillating cylinders, in certain cases, *swinging* of wake from side-to-side, around the center line and *mode competition* between various modes of vortex shedding is observed. Some of these features of the non-linear fluid–structure interaction are quite sensitive to the Reynolds numbers. The trajectory of the oscillating cylinder shows very interesting patterns including the well-known *Lissajou* figure of *8*. Several mechanisms of the non-linear oscillator for self-limiting its vibration amplitude are observed. As the vibration amplitude increases, the flow changes and so do the aerodynamic forces acting on the cylinder, to limit the amplitude of oscillations. The phenomenon of soft lock-in is also a mechanism of the oscillator to self-limit its oscillation amplitude and is typically observed for light cylinders that exhibit high-amplitude vibrations.

ACKNOWLEDGMENTS

Partial support for this work has come from the Department of Science and Technology, India under the project number DST-AE-95279 with Department of Aerospace Engineering, IIT, Kanpur.

REFERENCES

1. G. H. KOOPMANN 1967 *Journal of Fluid Mechanics* **28**, 501–512. The vortex wakes of vibration cylinders at low Reynolds numbers.
2. O. M. GRIFFIN, R. A. SKOP and G. H. KOOPMANN 1973 *Journal of Fluid Mechanics* **54**, 235–249. The vortex-excited resonant vibrations of circular cylinders.
3. T. SARPKAYA 1979 *Journal of Applied Mechanics* **46**, 241–258. Vortex-induced oscillations: a selective review.
4. G. H. TOEBES 1969 *Journal of Basic Engineering* **91**, 493–505. The unsteady flow and wake near an oscillating cylinder.
5. O. M. GRIFFIN 1971 *Journal of Applied Mechanics* **38**, 729–738. The unsteady wake of an oscillating cylinder at low Reynolds number.
6. Y. TANIDA, A. OKAJIMA and Y. WATANABE 1973 *Journal of Fluid Mechanics* **61**, 769–784. Stability of a circular cylinder in uniform flow or in a wake.
7. O. M. GRIFFIN and S. E. RAMBERG 1975 *Journal of Fluid Mechanics* **75**, 257–271. Vortex shedding from a cylinder vibrating in line with an incident uniform flow.
8. R. KING 1977 *Ocean Engineering* **4**, 141–171. A review of vortex shedding research and its application.
9. W. W. DURGIN, P. A. MARCH and P. J. LEFEBVRE 1980 *Journal of Fluids Engineering, Transactions of the American Society of Mechanical Engineers* **102**, 183–190. Lower mode response of circular cylinders in cross-flow.
10. Y. LECOINTE, J. PIQUET and J. PLANTEC 1987 In *Forum on Unsteady Flow Separation* (K. N. Ghia, editor), FED-52, 147–157. *American Society of Mechanical Engineers*. Flow structure in the wake of an oscillating cylinder.
11. S. S. CHEN 1987 *Flow-Induced Vibrations of Circular Cylindrical Structures*. New York: Hemisphere Publishing Corporation.
12. C. H. K. WILLIAMSON and A. ROSHKO 1988 *Journal of Fluids and Structures* **2**, 355–381. Vortex formation in the wake of an oscillating cylinder.
13. D. J. OLINGER and K. R. SREENIVASAN 1988 *Physical Review Letters* **60**, 797–800. Nonlinear dynamics of the wake of an oscillating cylinder.

14. A. ONGOREN and D. ROCKWELL 1988 *Journal of Fluid Mechanics* **191**, 197–223. Flow structure from an oscillating cylinder Part 1. Mechanisms of phase shift and recovery in the near wake.
15. A. ONGOREN and D. ROCKWELL 1988 *Journal of Fluid Mechanics* **191**, 225–245. Flow structure from an oscillating cylinder Part 2. Mode competition in the near wake.
16. R. D. BLEVINS 1990 *Flow-Induced Vibration*. New York: Van Nostrand Reinhold.
17. S. MITTAL and T. E. TEZDUYAR 1992 *International Journal for Numerical Methods in Fluids* **15**, 1073–1118. A finite element study of incompressible flows past oscillating cylinders and airfoils.
18. S. MITTAL, A. RATNER, D. HASTREITER and T. E. TEZDUYAR 1991 *International Video Journal of Engineering Research* **1**, 83–96. Space–time finite element computation of incompressible flows with emphasis on flows involving oscillating cylinders.
19. K. S. CHANG and J. Y. SA 1992 *American Institute of Aeronautics and Astronautics Journal* **30**, 1331–1336. Patterns of vortex shedding from an oscillating circular cylinder.
20. S. MITTAL and V. KUMAR 1999 *International Journal for Numerical Methods in Fluids* **31**, 1087–1120. Finite element study of vortex-induced cross-flow and in-line oscillations of a circular cylinder at low Reynolds numbers.
21. T. E. TEZDUYAR, M. BEHR and J. LIOU 1992 *Computer Methods in Applied Mechanics and Engineering* **94**, 339–351. A new strategy for finite element computations involving moving boundaries and interfaces—the deforming-spatial-domain/space–time procedure: I. The concept and the preliminary tests.
22. T. E. TEZDUYAR, M. BEHR, S. MITTAL and J. LIOU 1992 *Computer Methods in Applied Mechanics and Engineering* **94**, 353–371. A new strategy for finite element computations involving moving boundaries and interfaces—the deforming-spatial-domain/space–time procedure: II. Computation of free-surface flows, two-liquid flows, and flows with drifting cylinders.
23. Y. SAAD and M. SCHULTZ 1986 *SIAM Journal of Scientific and Statistical Computing* **7**, 856–869. GMRES: a generalized minimal residual algorithm for solving nonsymmetric linear systems.
24. T. E. TEZDUYAR, S. MITTAL, S. E. RAY and R. SHIH 1992 *Computer Methods in Applied Mechanics and Engineering* **95**, 221–242. Incompressible flow computations with stabilized bilinear and linear equal-order-interpolation velocity–pressure elements.
25. S. MITTAL 1992 *Ph.D. thesis, University of Minnesota*. Stabilized space–time finite element formulations for unsteady incompressible flows. Involving fluid–body interactions.
26. H. SCHLICHTING 1979 *Boundary-Layer Theory*. New York: McGraw-Hill. Seventh edition.
27. S. BALACHANDAR and R. MITTAL 1996 Role of three-dimensionality in the near wake of two-dimensional cylinders. In *Mechanics and Thermal Sciences* (T. S. Mruthyunjaya, editor), Advances in Mechanical Engineering—Vol. II, 1385–1395, Indian Institute of Science Bangalore, India: Narosa Publishing House.
28. V. KALRO and T. TEZDUYAR 1995 Parallel finite element computation of 3D incompressible flows on MPPs. In *Solution Techniques For Large-Scale CFD Problems* (W. G. Habashi, editor), Computational Methods in Applied Sciences, New York: Wiley.
29. S. MITTAL 2001 *Physics of Fluids* **13**, 177–191. Computation of three-dimensional flows past circular cylinder of low aspect-ratio.
30. C. H. K. WILLIAMSON 1996 *Annual Review of Fluid Mechanics* **28**, 477–539. Vortex dynamics in the cylinder wake.
31. O. M. GRIFFIN and S. E. RAMBERG 1982 *Journal of Energy Resources Technology, Transactions of the American Society of Mechanical Engineers* **104**, 2–13. Some recent studies of vortex shedding with application to marine tubulars and risers.
32. M. BEHR 1992 *Ph.D. thesis, Department of Aerospace Engineering, University of Minnesota*. Stabilized finite element methods for incompressible flows with emphasis on moving boundaries and interfaces.